Experimental Setup to Compare Measurements and Numerical Simulations in Magnetic Resonance Imaging RF Dosimetry

Published paper @DOI: 10.1109/TIM.2017.2687138

Experimental set-up to compare measurements and numerical simulations in Magnetic Resonance Imaging RF dosimetry

U. Zanovello, M. Borsero, D. Giordano, L. Zilberti, F. Maggiorelli and G. Tiberi

***Abstract* — Many of the parameters associated with the Magnetic Resonance Imaging (MRI) antennas are estimated by means of numerical simulations. Taking into account the unavoidable numerical approximations and imperfections of the models, an experimental validation of the theoretical results becomes essential. This work describes three measuring set-ups which allow the comparison between measurements of electromagnetic fields and the same quantities computed numerically. The experimental activity highlighted some critical aspects of the numerical results that could bring to a wrong estimation of the parameters associated with the MRI antennas. Results suggest the importance and feasibility of a dosimetry experimental set-up suitable for MRI antennas characterization.**

***Index Terms* —Magnetic Resonance Imaging, MRI antennas, MRI dosimetry, Field probes, RF Electromagnetic Measurements.**

I. INTRODUCTION

MAGNETIC resonance imaging (MRI) is an imaging technique used primarily in medical settings to produce high quality images of the inside of the human body. MRI is clearly a growing science, it has a wide range of applications in medical diagnostics and over 25000 scanners are estimated to be in use worldwide. Even though MRI is a safe technique, the number of accidents causing patient damage has risen.

One of the most important and indicative parameters associated with the safety of a human body subjected to radiofrequency (RF) radiation is the "specific absorption rate" (SAR) of energy developed by the electromagnetic field in the tissues, per mass unit.

$$SAR = \frac{1}{M}\int_{Mass} \frac{\sigma(P)E(P)^2}{\rho(P)}\,dm \quad \left(\frac{W}{kg}\right) \tag{1}$$

where:

$\boldsymbol{E}(\boldsymbol{P})$ is the electric field in point P of tissue (V/m)
$\boldsymbol{\rho}(\boldsymbol{P})$ is the mass density in point P of tissue (kg/m^3)
$\boldsymbol{\sigma}(\boldsymbol{P})$ is the electrical conductivity in point P of tissue (S/m)
$\boldsymbol{M}$ is the averaged mass (kg)

Documents [1], [2] distinguish between the local SAR, averaged over the mass of 10 g, and global SAR averaged over the whole body. Different limits have been established for the two quantities, in function of the exposure time, both for patients and operators.

Whereas the global SAR can be estimated by the active power flowing through the coils of the MRI tomograph, the only way to have a satisfactory idea of the local SAR is by means of numerical simulations.

Considering the strictly relation of SAR with the electric field (see (1)) generated by the MRI coils inside the tissues, the importance of such field measurements to validate the numerical results becomes evident.

On the other hand, there are several parameters describing the coils efficiency based on the magnetic field. For example the transmit efficiency is defined as the ratio between the clockwise rotating magnetic field and the square root of the active power flowing through the coil. Furthermore, in order to avoid artifacts in the final MRI image, it is essential to ensure a magnetic field inside the region of interest (ROI) as

This paragraph of the first footnote will contain the date on which you submitted your paper for review. It will also contain support information, including sponsor and financial support acknowledgment. For example, "This work was supported in part by the U.S. Department of Commerce under Grant BS123456".

U. Zanovello is a Ph.D. student in Electrical, Electronic and Telecomunications engineering at Politecnico di Torino (I-10129 Torino, Italy). He develops his activity in cooperation with the Istituto Nazionale di Ricerca Metrologica (I-10135 Torino, Italy) (e-mail: u.zanovello@inrim.it).

M:Borsero, D. Giordano and L. Zilberti are with the Istituto Nazionale di Ricerca Metrologica (I-10135 Torino, Italy) (e-mail: l.zilberti@inrim.it; d.giordano@inrim.it; m.borsero@inrim.it)

F. Maggiorelli is with Dipartimento di Scienze Fisiche, della Terra e dell'Ambiente, Università di Siena and with Istituto Nazionale di Fisica Nucleare (INFN), Sezione di Pisa (e-mail: g.tiberi@iet.unipi.it)

G. Tiberi is with the Laboratory of Medical Physics and Biotechnologies for Magnetic Resonance, IRCCS Stella Maris Foundation, Pisa, Italy and with Imago7 Foundation, Pisa, Italy (e-mail: maggesca@gmail.com)

homogeneous as possible. From these considerations grows the benefit to provide an experimental characterization of the coil also in terms of the generated magnetic field.

For these reasons, an MRI dosimetry set-up for RF electromagnetic measurements has been designed and realized at the Istituto Nazionale di Ricerca Metrologica (INRIM). The experimental set-up is composed of a cylindrical polycarbonate phantom filled with a tissue-simulating liquid (TSL), prepared by ZurichMedTech [3], whose electric proprieties (i.e. electric permittivity and electrical conductivity) are comparable to those of human tissues. All the measurements have been acquired along predefined investigating lines inside the phantom thanks to an automatic tri-axial positioning system (gantry).

The present paper is an extension of the work presented for the CPEM 2016 Digest (Proceedings) [4] and proposes the comparison between numerical results and experimental acquisitions for three different loop coils.

The set-up section is divided in three parts. In the first subsection, measurements have been carried out generating the electromagnetic field with a well-known coil already characterized with a previous set-up [4, 5]. Although the coil, i.e. the antenna, was not designed to work inside a real MRI tomograph, it has been tuned to work at 128 MHz that is a common frequency in MRI and represents the 1H-Larmor frequency associated to 3 T static magnetic fields.

In the second subsection, measurements have been performed with a real MRI coil. The coil was provided by the "Imago 7" Foundation (Pisa, Italy) and all the measurements have been carried out at INRIM. The antenna was double tuned at the frequencies of 79 MHz and 298 MHz that correspond to the Larmor frequencies of the 23Na and 1H associated to a 7 T static magnetic field, respectively.

In the third subsection, it is provided a detailed description of a volume coil ("Birdcage" coil) that has been designed at INRIM and will be the object of future work.

II. SET-UP

A. First experimental set-up

A first experimental set-up (Fig.1) has been used to perform measurements generating the fields by means of a well-known antenna designed and realized at INRIM. The coil had already been characterized with a previous experimental set-up based on a manual positioning system [5]. In this sub-section the old positioning system has been replaced by a new automatic tri-axial robot ("gantry"). A new GUI-based management software has been developed through the so-called "python-QT" bindings. The program handles both the acquisition and generation processes and allows to control the gantry movement in different ways. A new TSL liquid [3], in which all the measurements have been performed, has replaced the previous one with slightly different electric proprieties. Finally, a new electric field probe, calibrated inside the actual TSL, has been used to perform the electric field measurements.

The main aim of this acquisition phase was to validate the new set-up and to develop an accurate measuring model that takes into account all the possible contributions that concur to the uncertainty of the measurand. An accurate description of the measuring model and of the uncertainties propagation is provided in Appendix A.

Fig.1: First experimental set-up

The considered experimental set-up was hence composed of a cylindrical phantom, of radius equal to 125 mm and height equal to 250 mm, filled with the TSL almost up to the edge.

The liquid was characterized by an electric permittivity ε_r equal to 78 and an electrical conductivity σ equal to 0.47 S/m (all the parameters have been provided with the liquid by ZurichMedTech). The phantom was placed on a dielectric support (height equal to 50 cm) on which also the coil has been positioned. The coil supply has been generated with a "ROHDE & SCHWARZ Vector Signal Generator-SMW200A" amplified by a "BONN Elektronik BSA 0110-100 W amplifier". The synthesizer frequency range is from 100 kHz to 3 GHz whereas the amplifier bandwidth is 100 kHz to 400 MHz with a gain of about 60 dB. The INRIM coil is made of an active rectangular wire (110 mm × 110 mm) surrounded by a metal shield. The shield presents a gap, covered by an aluminum sheet, to avoid blocking the intentional coupling between probe and field to be measured [6]. The coil has been tuned to 128 MHz by means of proper capacitors connected in series to the supply.

Since the electromagnetic field measurement should be performed in the near-field region, where the spatial field gradient is relatively large, RMS isotropic field probes with very small dimensions have been chosen [7]. Moreover, owing to their use inside the phantom, resistance to organic solvent must be guaranteed. Both the electric and magnetic field probes have been connected to their remote unit by means of an optic fiber to avoid measurement interferences. The remote unit has been managed by the PC thanks to a LAN cable connection.

The measurements have been performed along 4 vertical lines inside the TSL and, for each line, a set of 37 acquisitions (5 mm spaced) has been carried out. The four lines are

100 mm, 80 mm, 60 mm and 40 mm distant from the center of phantom towards the antenna. Thanks to the gantry and to the software "lines acquisition" function, every set of measurements lasted no more than 5 minutes. After that, the results have been compared with numerical simulations. In a simulation environment (CST-MWS©) the physical set-up has been properly modeled and simulated with the frequency-domain solver. The numerical results have been extracted along the same lines on which the measurements have been carried out. For each experimental acquisition, the active power flowing through the coil has been acquired thanks to a reflectometric power measurement method. By means of a bi-directional coupler "BONN Elektronik BDC 0125 40-250" associated with two power meters "Rohde&Schwarz NRP-Z51", it has been possible to evaluate the incident and reflected power to the coil and, hence, the actual power flowing through. For each line, the mean power has been computed and it has been used as driving term for the corresponding simulation.

B. Second experimental set-up

A second set of measurements has been carried out generating the RF electromagnetic field with a double-tuned planar coil instead of the previous one. The coil was provided by the "Imago 7" Foundation and it was designed to work in a real 7 T tomograph. The antenna consists of two concentric rectangular loops with independent supply (Fig.2). For both the loops, the angles are blended with 28 mm curvature radius. The loops are etched on an FR4 printed circuit board with 200 µm thickness and are plunged in a mechanic support made of polylactide (PLA) thermoplastic (Fig.3).

The external loop (110 mm x 110 mm) is tuned at 298 MHz in order to stimulate the 1H nuclei response under a 7 T static magnetic field. Considering the short wavelength at this frequency, 7 tuning capacitors are distributed along the loop at the same distance from each other.

The internal loop (85 mm x 95 mm) is tuned at 79 MHz in order to stimulate the 23Na atoms response under a 7 T static magnetic field. In this case, taking into account the smaller dimension and greater wavelength, only 3 tuning capacitors are used.

At the 23Na frequency of 79 MHz, the 1H loop presents a high impedance ensuring a good decoupling with the Sodium coil. On the contrary, the 23Na loop shows a low impedance at the 1H frequency. To decouple the loop also at 298 MHz, a

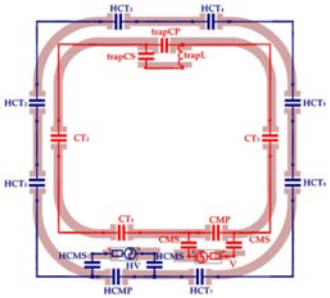

Fig.2: Double-tuned 1H/23Na planar antenna electrical scheme

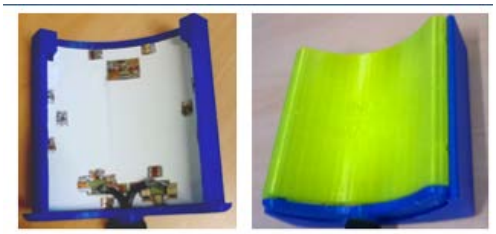

Fig.3: Double-tuned 1H/23Na planar antenna polylactide (PLA) thermoplastic mechanic support

"trap" circuit is inserted on the Sodium coil. The "trap" consists of a 298 MHz resonating LC circuit that has the effect to open the Sodium loop avoiding the coupling at this frequency between the two loops.

Both the coils are matched to 50 Ω with a capacitive matching network and the supply symmetry is ensured by the use of "baluns".

Clinical practice for this double-tuned antenna requires that the 1H loop be used only as "localizer". When the correct placement is found, the 23Na loop is employed in order to obtain the required 23Na image [8].

The coil has been fixed to the phantom thanks to some paper tape being careful to maintain the loop in a vertical position and central to the phantom height.

Also in this case, electrical and magnetic field measurements have been performed along the same lines defined in the previous subsection with 37 acquisition for each line.

Since the magnetic and electric field probes are not calibrated at 298 MHz and the TSL is not characterized for this frequency, all the measurements have been carried out for the Sodium coil at 79 MHz. Furthermore it should be underlined that, considering the reduced application of this hydrogen coil used only with a "localizer" function, there is no practical interest to investigate its behavior in detail. Concerning an experimental activity at 298 MHz, electromagnetic field measurements will be the subject of a future work where the fields will be generated with an antenna specifically designed for an extensive use at this frequency.

The set-up has been left unchanged with respect to the previous sub-section and the experimental results have been compared to numerical results. Also in this case, the simulations have been computed with the frequency-domain solver of CST-MWS© and the numerical results have been extracted along the same investigated lines.

C. Third experimental set-up

A third experimental set-up is now under realization at INRIM. It contemplates the use of a volume coil, the "Birdcage" coil, to generate the electromagnetic fields inside the cylindrical phantom filled with the TSL. Birdcage resonators are the typical antennas involved in the RF electromagnetic field generation in MRI and are designed to feature a homogenous circular polarized magnetic field inside their volume [9] (Fig.4).

In particular a high-pass 16-legs birdcage resonator coil has been designed. The coil is 460 mm high with a 320 mm

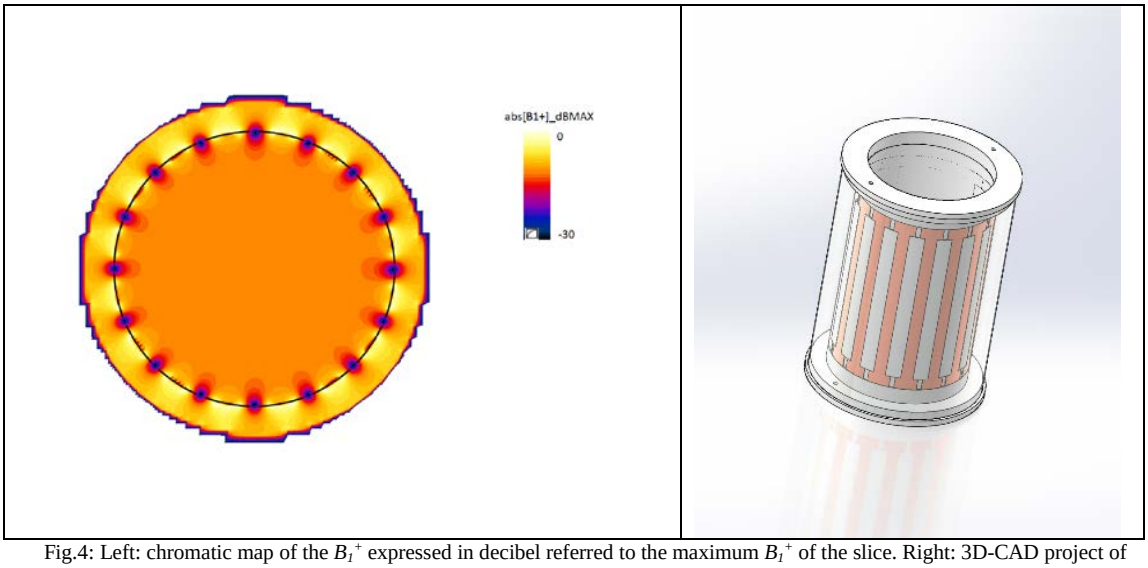

Fig.4: Left: chromatic map of the B_1^+ expressed in decibel referred to the maximum B_1^+ of the slice. Right: 3D-CAD project of the 16-legs Birdcage high-pass coil designed at INRIM

diameter. The conductive circuit of 70 µm thickness is printed on a 0.2 mm thickness PCB support. For a 16-legs high-pass birdcage, 32 capacitors, whose capacitance determines the tuning frequency of the coil, must be provided. Each couple of capacitors links one leg to the next; one in the upper side and the other in the bottom. The birdcage is tuned to 128 MHz (a common frequency in MRI that represents the 1H-Larmor frequency associated to 3 T static magnetic field) and it is designed to be fed in quadrature operation. Finally, a 600 mm height, 350 mm diameter copper shield surrounds the coil. The shield is maintained in the desired position thanks to two plugs fixed on the PCB support (Fig.4).

In order to evaluate the capacitance values that ensure a correct tuning of the antenna, some simulations have been carried out with a FDTD (Finite Difference Time Domain) solver (Sim4Life©) developed by ZurichMedTech. A 24 pF capacitance has been chosen as correct value to guarantee an highly homogenous clockwise rotation magnetic field (B_1^+). Some variable capacitors have been contemplated in order to allow fine tuning and matching procedures during the experimental application. High voltage ($V_{DC} = 1000\,V$) RF surface-mount multilayer ceramic capacitors and high voltage ($V_{DC} = 500\,V$) RF film dielectric trimmers capacitors have been purchased from the VISHAY manufacturer. The variable capacitors are characterized by a capacitance range from 5 pF to 57 pF that perfectly fits the needs of the actual application.

Finally, in order to evaluate also the phase of the acquired electromagnetic field (allowing, among others, to evaluate the correct polarization of the RF magnetic field generated by the birdcage coil), new concept time-domain probes have been acquired [7].

III. Results and Discussion

In this section, some of the results obtained during the experimental activity are proposed and discussed. As explained in the previous section, electric and magnetic field measurements have been made along 4 vertical lines inside the

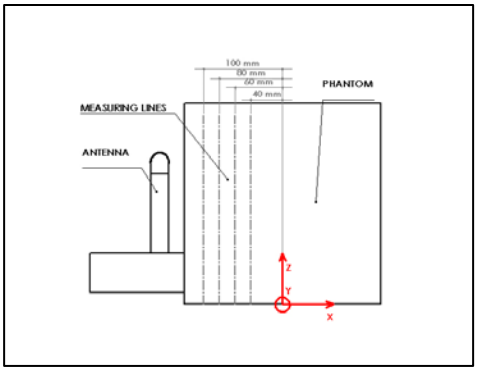

Fig.5: Reference coordinate system and measuring lines for the experimental set-up. In the picture the antenna used for the first experimental set-up is shown (side view)

TSL and, for each line, a set of 37 acquisitions (5 mm spaced) has been carried out. The four lines are 100 mm ("line-100"), 80 mm ("line-80"), 60 mm ("line-60") and 40 mm ("line-40") distant from the center of phantom towards the antenna, respectively. In the first sub-section the acquisitions carried out with the first experimental set-up (refer to the "set-up" section) are reported and compared with the corresponding numerical simulation results. In the second subsection, all the proposed comparisons refer to the second experimental set-up. The z-coordinate in all the following figures should be intended as growing from the phantom base to the top. The x-axis is parallel to the longitudinal axis of the loop antenna and the y-axis remains parallel to the plane of the coil as shown in Fig.5.

In this section, only the results of the measurements along the lines evaluated to be more interesting are reported. The uncertainty bars shown in the figures refer to the expanded uncertainty associated to the corresponding acquisition (see Appendix A).

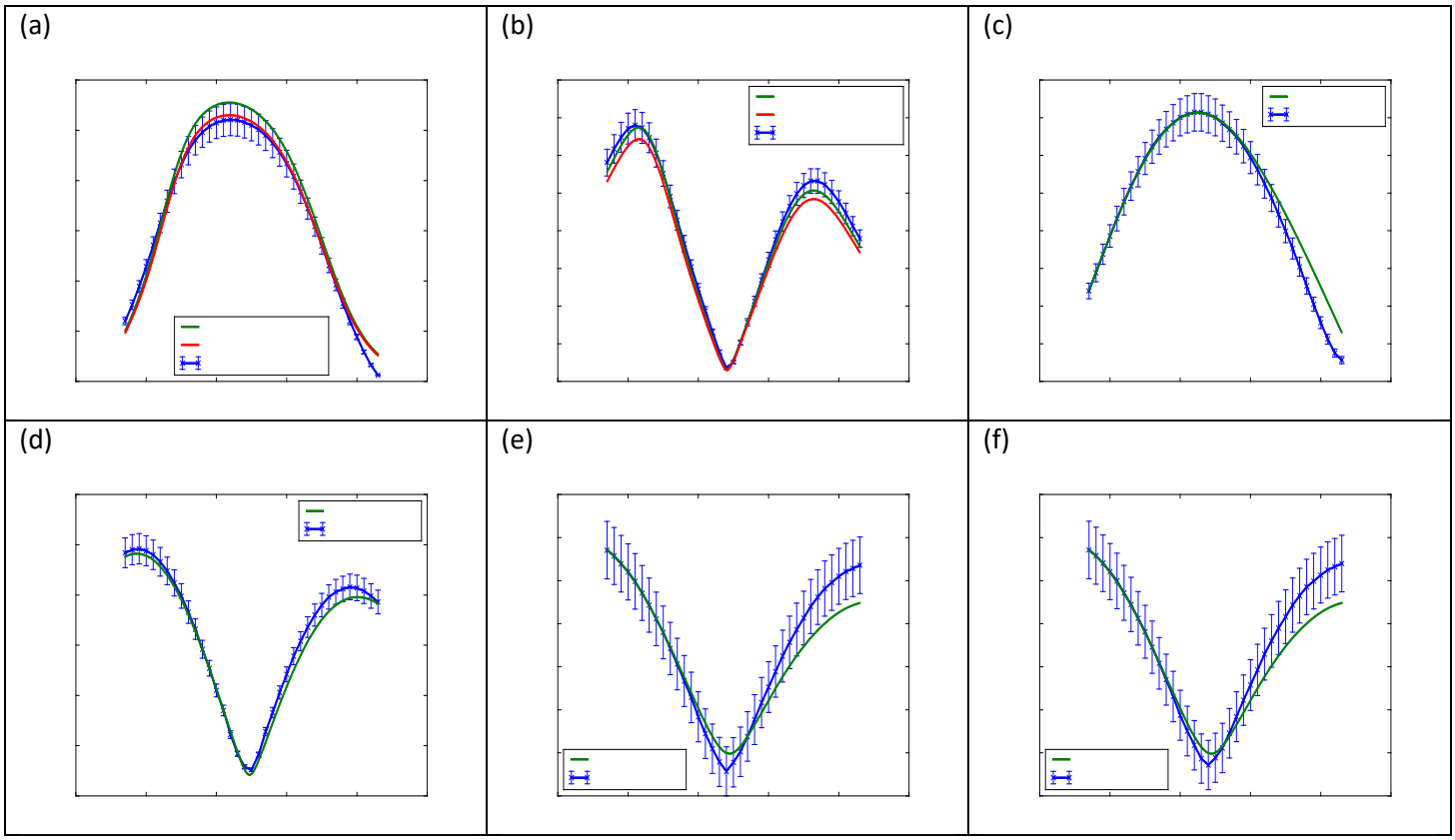

Fig.6: Comparison between the experimental results obtained with the first experimental set-up and the numerical simulations. The comparison is reported for the magnetic field along the" line-100" (a,b) and along the "line-40" (c,d) both for the z-component and for the xy-component. The comparison for the electric field is reported for "line-40" both for the xy-component and for the field magnitude (e,f).

A. First experimental set-up

In the first experimental set-up the antenna has been supplied with a net active power (the power incident to the coil minus the reflected one) equal to 15 W. In this set-up, the center of the coil corresponds to a z-coordinate equal to 120 mm.

The comparisons of the xy-component (H_{xy}) and of the z-component (H_z) of the magnetic field at 128 MHz between the experimental acquisitions and the numerical results are reported in Fig.6(a, b, c, d). In Fig.6(a, b) the acquisitions have been carried out along the "line-100" whereas in Fig.6(c, d) the investigated line is the "line-40". The results are found to be satisfactory for all the four presented cases. In Fig.6(a, b) it is highlighted the high sensitivity of the magnetic field at near distances to internal conductor shape variations. In the INRIM coil the internal conductor is hidden by the external shield. It is hence almost impossible to evaluate its effective shape. The green lines represent a simulation where the rectangular shape of the internal wire has the vertices blended with a radius of 10 mm whereas those depicted in red with an angle of 5 mm. Differences are found to be appreciable especially on the peaks of the curves. In Fig.6(a) the 5 mm radius improves the results but has a negative effect on the z-component of the magnetic field (Fig.6(b)). The relative differences between the numerical results obtained with the two radii are muffled at greater distances. The simulation lines in all the other proposed results are to be intended with a "blend radius" equal to 10 mm. In Fig.6(c) the peaks difference notable in Fig.6(a) becomes negligible. However, some discrepancies between the two curves are found in the upper part of the "line-40". Aside from the modelling inaccuracies, these are presumably due to the very small magnetic field amplitudes. These magnetic field magnitudes are comparable with the field noise and the probe behavior could be unsatisfactory at these low signal levels. The agreement between the z-component of the measured magnetic field and the simulated results, depicted in Fig.6(b, d), is very appreciable and supports the correctness both of the experimental procedure and of the numerical model. The results for the electric field along the "line-40" are depicted in Fig.6(e, f).

In Fig.6(e) it is shown the comparison for the xy-component (E_{xy}) and in Fig.6(f) the comparison for the magnitude of the electric field. The agreement between the numerical and measurements curves is found to be satisfactory in both cases. Some disagreements between the curves are appreciable in Fig.6(e, f) in the upper part of the "line-40" where the acquired points are nearer the liquid surface. The shield effect of the TSL decreases in these points and the electric field noise (not predictable from simulations) of the environment could cause some discrepancy between measurements and numerical results. The similarity between the xy-component Fig.6(e) and the magnitude Fig.6(f) of the electric field, is not surprising considering the value of the z-component that is negligible as expected by theory.

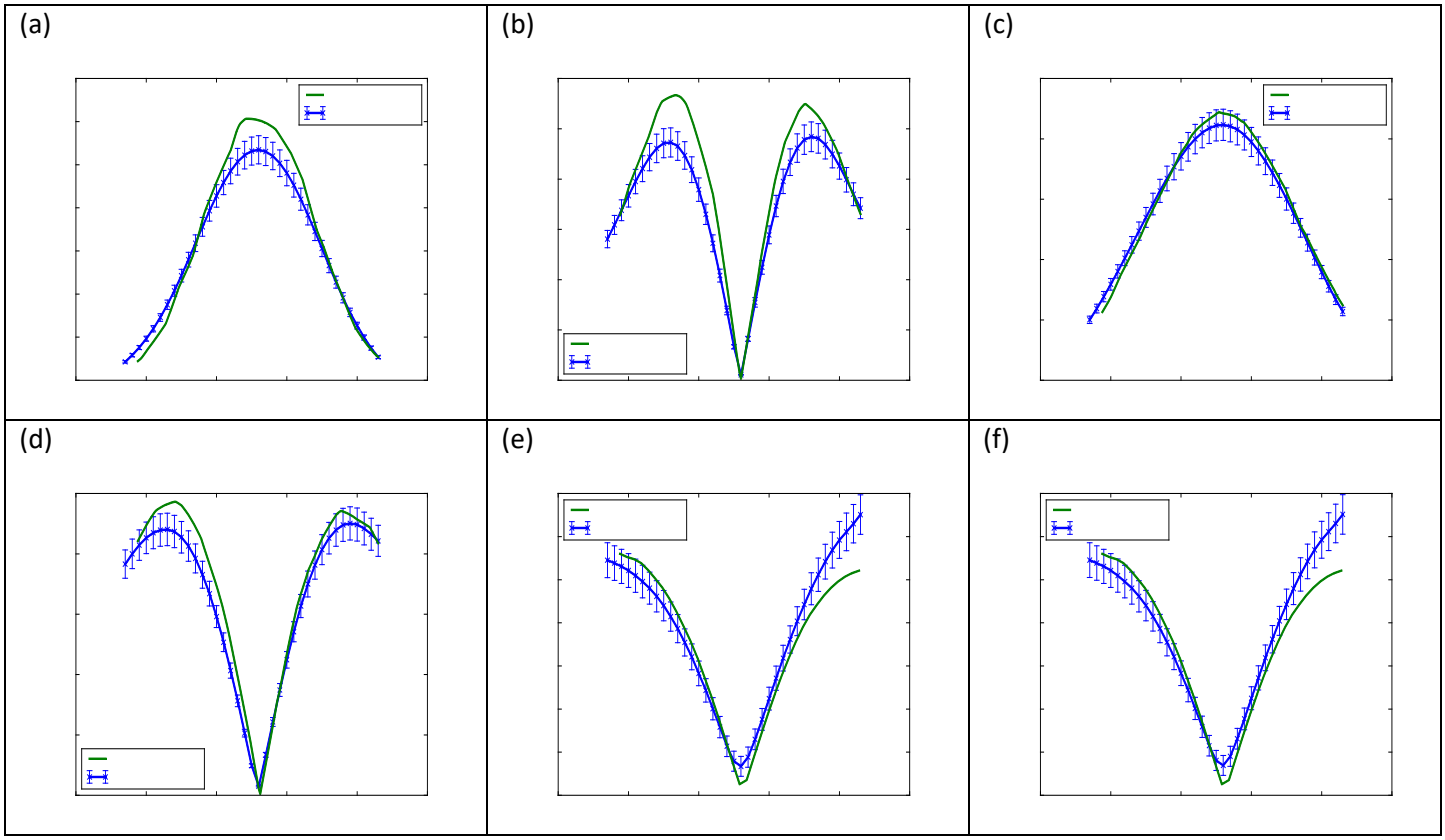

Fig.7 Comparison between the experimental results obtained with the second experimental set-up and the numerical simulations. The comparison is reported for the magnetic field along the" line-80" (a,b) and along the "line-40" (c,d) both for the z-component and for the xy-component. The comparison for the electric field is reported for "line-40" both for the xy-component and for the field magnitude (e,f)

Finally, considering the points where the measured electric or magnetic field values are different from those simulated, it is noticeable the importance of a proper characterization of the MRI-antennas to avoid, for example, possible underestimations of the SAR values or overestimations of the transmit efficiency.

B. Second experimental set-up

In the second set-up, the planar antenna, used to generate the electromagnetic field, has been supplied with a net power of 9.5 W. The results shown in this section refer to the sodium coil at 79 MHz.

The comparisons of the xy-component (H_{xy}) and of the z-component (H_z) of the magnetic field at 79 MHz between the experimental acquisitions and the numerical results are depicted in Fig.7(a, b, c, d). Fig.7(a, b) refer to measurements along the "line-80" and Fig.7(c, d) to those along the "line-40". Although the shape of the curves for measurements and simulations are similar, in Fig.7(a, b) it is appreciable a difference between the peak values both in the xy-component case and in the z-component one. This inconsistency is partially compensated considering a farther line as in Fig.7(c, d). As pointed out in the previous subsection, the electromagnetic field near the antenna could be highly influenced by any minimum shape variation of the model. Considering the unavoidable errors committed in the effort of reproducing the real experimental set-up in a simulation environment, some reasonable differences between experimental and numerical results should be taken into account. It should be noted that the magnetic field values obtained in this set-up are higher than those obtained with the first experimental set-up.

In Fig.7(c), at the upper part of "line-40", the relative errors between the experimental results and the numerical ones are smaller with respect to the previous set-up (see Fig.6(c)). This assumption could partially confirm the observation, highlighted in the previous sub-section, that the probe behavior is unsatisfactory at low magnetic field values.

The results for the electric field along the "line-40" are shown in Fig.7(e, f). In Fig.7(e) it is depicted the comparison for the xy-component (E_{xy}) and in Fig.7(f) the comparison for the magnitude of the electric field. The accordance between the numerical and experimental results is considered satisfactory for both Fig.7(e) and Fig.7(f). As for the results obtained with the first experimental set-up, also in this case some disagreements appear in the upper part of the "line-40" probably due to the weaker shield effect of the TSL.

The affinity between the measured values of the xy-component and the magnitude of the electric field is due to a measured z-component that is negligible as expected by theory.

Finally, also in this case, similar considerations concerning possible SAR underestimation or transmit efficiency overestimation can be applied for this antenna.

CONCLUSION AND DEVELOPMENTS

Some comparisons between numerical results and experimental measurements have been proposed. The experimental acquisitions have been carried out along specific lines in a liquid that simulates the electrical properties of human tissues. Such comparisons have been proposed with two different experimental set-ups. In the first set-up the electromagnetic fields have been generated with a well-known antenna designed and developed at INRIM. In the second set-up the fields have been generated with an antenna specifically designed for an MRI application and provided by the "Imago 7" Foundation (Pisa, Italy).

All the results have been analyzed in detail and several critical aspects have been highlighted. The absolute importance of a good experimental characterization that guarantees a correct estimation of all the parameters related to the electric and magnetic field generated (e.g. SAR, transmit efficiency etc.) has been put in evidence.

Future works include the extension of the calibration of the field probes and of the TSL electrical properties evaluation up to 300 MHz. After that, it will be possible to perform the characterization of a planar Hydrogen MRI coil.

Finally, the described "third experimental set-up" (birdcage antenna) will be completed and new electric and magnetic field measurements will be carried out and compared to numerical simulations.

APPENDIX A

Measurement model

In the following analysis all the contributions in the measurement model that introduce an uncertainty in the measurand are described in detail. The following considerations deal with the magnetic field but the same description can be applied also to the electric field. The uncertainty estimation and propagation is carried out taking into account the guidelines proposed by the JCGM 100:2008 (GUM) [10].

The measurement model is given by

$$H_{p_0,T_{liq_0},\tilde{P}} = H_{p,T_{liq},P} + C_{cal} + C_{\Delta M} + \\ + C_{\Delta T_{liq}} + C_{\delta \mathrm{pow}(\Delta T_{ins})} \qquad \text{(A.1)}$$

where:

$\boldsymbol{H_{p_0,T_{liq_0},\tilde{P}}}$ represents the best estimate of the magnetic field in the point "p_0", at the liquid temperature "T_{liq_0}" and at the power "$\tilde{P}$" flowing through the coil, evaluated at the mean power of all the acquisitions along a specific line

$\boldsymbol{H_{p,T_{liq},P}}$ represents the observed quantity, read from the instrument display, in the actual point "p", at the actual liquid temperature "T_{liq}" and at the actual supply power "P". Only one reading has been done for each point of acquisition so $\widetilde{H_{p,T_{liq},P}} = H_{p,T_{liq},P}$

$\boldsymbol{C_{cal}}$ takes into account the effect of the calibration coefficient, associated with the specific field probe, on the measurand. It has been evaluated that C_{cal} does not contribute to significant errors indeed the estimated value has been considered zero so $\widetilde{C_{cal}} = 0$

$\boldsymbol{C_{\Delta M}}$ takes into account the positioning error that is the difference from the actual acquisition position "p" and the desired position "p_0". It has been evaluated that $C_{\Delta M}$ does not contribute to significant errors indeed the estimated value has been considered zero so $\widetilde{C_{\Delta M}} = 0$

$\boldsymbol{C_{\Delta T_{liq}}}$ takes into account the effect of the temperature oscillation on the electric properties of the liquid that is the difference from the actual liquid temperature "T_{liq}" and the desired one "T_{liq_0}". Since we are not able to measure the exact liquid temperature, we can't take into account any significant effect of $C_{\Delta T_{liq}}$ on the measurand. Indeed the estimated value has been considered zero so $\delta_{rep}\widetilde{(\Delta T_{liq})} = 0$

$\boldsymbol{C_{\delta \mathrm{pow}(\Delta T_{ins})}}$ takes into account the difference from the actual power flowing through the coil "P" and the mean power used in the simulations "$\tilde{P}$". During the line acquisition procedure, the supply voltage is set by the generator but the real supply voltage depends on the instrument temperature "T_{inst}" and so does the real power in the coil. It has been evaluated that $C_{\delta \mathrm{pow}(\Delta T_{ins})}$ does not contribute to significant errors indeed the estimated value has been considered zero so $\widetilde{H_{p,T_{liq},P}} = 0$

As prescribed by the GUM, at each of the previous contributions, it is associated a pdf (probability density function) based on the available knowledge of the quantity itself. In the following list the procedure is described in detail.

$\boldsymbol{H_{p,T_{liq},P}}$ is affected by the uncertainty due to the device resolution. The instrument resolution is 0.001 A/m and hence a rectangular distribution with limits $a = H_{p,T_{liq},P} - 0.0005$ and $b = H_{p,T_{liq},P} + 0.0005$ would be used to characterize the knowledge of the quantity. The associated uncertainty is $u(H_{p,T_{liq},P}) = \frac{b-a}{\sqrt{12}} = 0.0003\,\frac{A}{m}$. For the electric field probe, the uncertainty associated to this parameter has been evaluated to be $\frac{1}{\sqrt{3}} = 0.58\,\frac{V}{m}$. This higher value is due to the high noise level detected during such field measurements

$\boldsymbol{C_{cal}}$ is affected by the uncertainty provided by the probe calibration certificate. It is said that the calibration factor influences the read value in a Gaussian way with an expanded uncertainty equal to 10% of the read field value with a 95% confidence interval. The associated uncertainty is $u(C_{cal}) = \frac{0.06}{1.96} H_{p,T_{liq},P} = 0.05 H_{p,T_{liq},P}\,\frac{A}{m}$

$\boldsymbol{C_{\Delta M}}$ does not contribute to the measurand uncertainty. This assertion came from a set of 100 acquisitions developed in the following way. A measurement point characterized by a high position gradient field has been individuated in order to maximize the effect of the positioning error on the field reading. Before every acquisition the gantry has been forced to return in the origin of its axis and the quantity $\frac{H_{p,T_{liq},P}}{\sqrt{P}}$ has

been computed in order to avoid the effect of $C_{\delta\mathrm{pow}(\Delta T_{ins})}$ on the positioning error. The standard deviation of the distribution results to be negligible compared to all the other uncertainty contributions.

$\boldsymbol{C_{\Delta T_{liq}}}$ takes into account the uncertainty associated to the actual liquid temperature T_{liq}. It is known that the laboratory temperature is (24 ± 3) °C and it is foreseeable that also the liquid temperature will change in the same range (21 to 27 °C). For a temperature variation within this range, the maximum difference in terms of field amplitude has been estimated to be less than 2% of the read field amplitude. Hence, a rectangular distribution with limits $a = (1 - 0.01)H_{p,T_{liq},P}$ and $b = (1 + 0.01)H_{p,T_{liq},P}$ would be used to characterize knowledge of the quantity. The associated uncertainty is $u\left(C_{\Delta T_{liq}}\right) = \frac{b-a}{\sqrt{12}} = 0.006H_{p,T_{liq},P}\frac{A}{m}$

$\boldsymbol{C_{\delta\mathbf{pow}(\Delta T_{ins})}}$ takes into account the uncertainty associated to the power flowing through the coil statistically different from its mean value used to obtain the numerical results. In order to evaluate this effect, 80 consecutive acquisitions (corresponding to acquire consecutively two lines) have been carried out without moving the gantry. Considering the temperature variation of the instruments from the first to the last acquisition, the maximum difference in terms of read field amplitude has been estimated to be less than 2% of the read field amplitude. Hence, a rectangular distribution with limits $a = (1 - 0.01)H_{p,T_{liq},P}$ and $b = (1 + 0.01)H_{p,T_{liq},P}$ would be used to characterize knowledge of the quantity. The associated uncertainty is $u\left(C_{\delta\mathrm{pow}(\Delta T_{ins})}\right) = \frac{b-a}{\sqrt{12}} = 0.006H_{p,T_{liq},P}\frac{A}{m}$.

Table 1 summarizes all the previous contributions. For each quantity in (A.1) the associated pdf, the mean value of the quantity (μ) and the standard deviation (σ) are shown

Quantity	PDF	Parameters	
		μ	σ
$H_{p,T_{liq},P}$	R(a,b)	$H_{p,T_{liq},P}$	$0.0003\frac{A}{m}$
C_{cal}	N(μ,σ²)	0	$0.05H_{p,T_{liq},P}\frac{A}{m}$
$C_{\Delta M}$	*	0	$0\frac{A}{m}$
$C_{\Delta T_{liq}}$	R(a,b)	0	$0.006H_{p,T_{liq},P}\frac{A}{m}$
$C_{\delta\mathrm{pow}(\Delta T_{ins})}$	R(a,b)	0	$0.006H_{p,T_{liq},P}\frac{A}{m}$

Table 1: Summary table for the assignment of the probability distributions

The model linearization is taken into account to propagate the uncertainty to the measurand as suggested by the GUM. The uncertainty associated to the measurand is hence expressed by

$$u(H_{p_0,T_{liq_0},\bar{P}}) = \sqrt{\sum_n s_n^2\, u^2(x_n)} \qquad \text{(A.2)}$$

where s_n with n=1,2..,4 represents the sensitivity coefficient computed as

$$s_n = \frac{df(x_1, \dots, x_n)}{dx_n} = 1\ \forall n \qquad \text{(A.3)}$$

with f representing the function defined in (A.1) and x_n is the quantity to which the sensitivity coefficient is referred to in the uncertainties propagation law (A.2).

Finally, since $u^2(H_{p,T_{liq},P})$ is much larger than any single component $u(x_n)$ from a non-normally distributed x_n, it is possible to apply the Central Limit Theorem. The coverage factor $k_{0.95}$ is equal to 1.960 for a normal distribution. The expanded uncertainty referred to the measurand $H_{p,T_{liq},P}$ is therefore:

$$U(H_{p_0,T_{liq_0},\bar{P}}) = 1.960 * u(H_{p_0,T_{liq_0},\bar{P}}) \qquad \text{(A.4)}$$

REFERENCES

[1] ICNIRP - International Commission on Non-Ionizing Radiation Protection, *Exposure to high frequency electromagnetic fields, biological effects and health consequences (100 kHz-300 GHz)*, 2009.

[2] IEC - International Electrotechnical Commission, *IEC 60601-2-33:2010+A1:2013+A2:2015 - Medical electrical equipment - Part 2-33: Particular requirements for the basic safety and essential performance of magnetic resonance equipment for medical diagnosis*, 2015.

[3] ZurichMedTech, «TLe78c0.47@64 (Liquid Simulating Averaged Tissue Parameters),» [Online]. Available: http://www.zurichmedtech.com/validation-hw/tsm/tle78c0-47-64/.

[4] U. Zanovello, L. Zilberti, M. Borsero e D. Giordano, «Experimental set-up to compare measurements and numerical simulations in Magnetic Resonance Imaging RF Dosimetry,» in *CPEM 2016 Digest*, Ottawa, Canada, Jul 11-15, 2016.

[5] O. Bottauscio, A. Cassarà, J. Hand, D. Giordano, L. Zilberti, M. Borsero, M. Chiampi e G. Weidemann, «Assesment of computational tools for MRI RF dosimetry by comparison with measurements on a laboratory phantom,» *Phys. Med. Biol.*, vol. 60, pp. 5655-5680, 2015.

[6] C. Carobbi e L. Millanta, «Analysis of the Common-Mode Rejection in the Measurement and Generation of Magnetic Fields Using Loop Probes,» *IEEE Transaction on Instrumentation and Measurement*, vol. 53, n. 2, April 2004.

[7] SPEAG, «SPEAG/PRODUCTS,» [Online]. Available: http://www.speag.com/products/easy4-mri/easy4-systems/; http://www.speag.com/products/tds/tds-time-domain-sensor-systems/.

[8] J. D. Kaggie, F. Maggiorelli, F. Riemer, M. McLean, L. Biagi, G. Tiberi, A. Retico, G. Buonincontri, F. Gallagher, M. Graves e M. Tosetti, «7 T Sodium/Proton Knee Imaging: First Results,» in *ISMRM UHF Symposium*, 2016.

[9] N. De Zanche, «Volume Coils,» in *RF Coils for MRI*, Wiley, 2012, pp. 123-136.

[10] BIPM Working Group 1 of the Joint Committee for Guides in Metrology (JCGM/WG 1), «JCGM 100:2008 - Evaluation of measurement data — Guide to the expression of uncertainty in measurement,» BIPM, Paris, 2008.